Engineering Science and Technology, an International Journal 24 (2021) 524–532

HOSTED BY

Contents lists available at ScienceDirect

Engineering Science and Technology, an International Journal

journal homepage: www.elsevier.com/locate/jestch

Full Length Article

Effect of sliding wear and electrochemical potential on tribocorrosion behaviour of AISI 316 stainless steel in seawater

Sabri Alkan [a,*], Mustafa Sabri Gök [b]

[a] Bartın University, Vocational School of Higher Education, Bartın 74100, Turkey
[b] Bartın University, Engineering Faculty, Bartın 74100, Turkey

ARTICLE INFO

Article history:
Received 17 February 2020
Revised 4 May 2020
Accepted 5 July 2020
Available online 10 August 2020

Keywords:
AISI 316
Tribocorrosion
Sliding wear
Corrosion
Seawater

ABSTRACT

Sliding tribocorrosion behaviours of AISI 316 stainless steel were investigated against alumina ball in natural seawater environment (SWE) under 5 N loads. OCP (open circuit potential), potentiostatic (−1 V and 0.3 V) and potentiodynamic measurements were enforced to understand the influence of the sliding wear and electrochemical potential on tribocorrosion behaviours of AISI 316 stainless steel in SWE. Tribocorrosion experiments were conducted with a ball-on-disk type reciprocating tribometer integrated with the three-electrode potentiostat. The wear track surfaces were examined by scanning electron microscope (SEM), energy dispersive spectroscopy (EDS) and optical profilometry. Mechanical effects reduced corrosion potential under both OCP and potentiodynamic scans in tribocorrosion conditions. Ploughing effects on the wear track were evident at the OCP and −1 V potential because of the predominance of mechanical effects. Pits were determined to develop due to the formation of the galvanic couple between worn and unworn surfaces after the tribocorrosion test, which was conducted under 0.3 V potential. The reduction of the contact area because of the pits and the lubricating effect of the oxides on the surface caused the lowest coefficient of friction (COF) in the wear zone at 0.3 V potential. Besides, COF obtained under −1 V cathodic protection potential (0.35) was less than in OCP condition (0.37) since it only occurred by the wear effects. The study also revealed that material loss from the wear track increased from cathodic potential towards anodic potential.

1. Introduction

Tribocorrosion consisting of tribology and corrosion sciences is an irreversible material transformation resulting from the simultaneous exposure of metals to mechanical and electrochemical effects within an electrolyte [1,2]. The marine industry is one of the important industries suffering from tribocorrosion because of the natural electrolyte property of seawater [3]. Various machinery, equipment and systems which operated under different dynamic wear conditions in seawater such as drilling equipment [4], wind and current turbines [5,6], some parts of ship main engines [7], ship anchor chains [8], piping systems [9], pumps [10], valves [11–13], propellers and shafts [14,15] are under the risk of tribocorrosion. Material losses and damages from tribocorrosion in marine machinery, equipment and systems occasionally lead to malfunctions, accidents, environmental pollutions, and consequently heavy operating cost [16,17]. For this reason, it is essential to determine the tribocorrosion behaviours of the machinery and equipment produced from metals operated in natural seawater environment (SWE).

Stainless steels are mostly preferred to produce marine equipment and systems. They show superior corrosion resistance thanks to a 1–3 nm thick passive oxide film layer that protects their surfaces against corrosion [18]. The susceptibility of stainless steels to some local types of corrosion, such as pitting and crevice corrosion in the SWE, is their weak side [16,19]. One of the most frequently used stainless steel types in the marine industry is AISI 316 due to its high mechanical and corrosion resistance. A few studies have been conducted so far about the tribocorrosion behaviours of AISI 316 stainless steel under sliding contact. Garcia et al. [20] found that the tribocorrosion behaviour of AISI 316 in sulfuric acid solution comprises two main stages. According to Garcia and colloquies, the passive oxide layer breaks down at the local points in the wear zone because of the mechanical interaction firstly and then a part of the wear zone where temporarily loses its passive character (active track area) is re-passivated again. Besides, Henry et al. [21] also reported when the load value is applied above a certain threshold value, it can break down the passive layer. Diomidis

* Corresponding author.
E-mail address: salkan@bartin.edu.tr (S. Alkan).
Peer review under responsibility of Karabuk University.

https://doi.org/10.1016/j.jestch.2020.07.004
2215-0986/

et al. [22] concluded that the passive film thickness in the wear track strongly increases the material loss and friction values. Mechanical effects disrupt the passive film layer under OCP which is leading to a significant reduction in corrosion potential [23,24]. Besides the behaviour of protective passive films, Panthiaux et al. [25] showed that it is possible to get information on corrosion rate, re-passivation, relationships between electrochemical reactions and friction in sliding contact zone using electrochemical techniques. Many researchers highlighted that the formation of the galvanic cell between wear track and unworn area could change the electrochemical status of surface and increase material loss for stainless steels [21,22,32–34,23,24,26–31]. Interaction between wear and corrosion named as synergism has a great effect of an increase of material losses in tribocorrosion [24,33,35–37]. Potentiostatic tests allow the measurement of wear induced corrosion of materials and wear-corrosion synergism [25,38]. The effect of anodic and cathodic potential on the coefficient of friction (COF) is also different. For example, Chen et al. [33] found the COF of the AISI 316 material against alumina (Al_2O_3) in the artificial SWE was reached the highest value in the cathodic potential and the smallest in the anodic potential. In another study conducted with AISI 316 by Obadele et al. [23], the loss of material resulting from tribocorrosion in artificial SWE is higher than in pure water environment. However, the corrosion-induced material loss was determined to be more dominant in material loss caused by tribocorrosion of AISI 316 stainless steel in the 3.5% NaCl solution in the same study. Recently, Holmes et al. [39] found that the increase in the load applied to the AISI 316 material and the penetration of the third bodies into the wear track zone in the micro-abrasion test which was performed in artificial saliva increased corrosion current density. Although many researchers were investigated tribocorrosion behaviour of AISI 316 in different electrolytes, the influence of sliding wear and electrochemical potential on the tribocorrosion behaviour of AISI 316 is still not well understood. It is necessary to understand friction, microstructure and material loss behaviour of AISI 316 under tribocorrosion conditions in natural seawater.

In this study, the effects of sliding wear and electrochemical potential on tribocorrosion behaviours of AISI 316 stainless steel in natural SWE were investigated comprehensively for the first time. In this context, OCP measurement, potentiostatic and potentiodynamic scans were enforced to understand tribocorrosion behaviours of AISI 316 in SWE. AISI 316 stainless steel was abraded against the alumina ball in natural SWE (2.38% NaCl) which was characterised by the method of inductive coupled plasma-optical emission spectroscopy (ICP-OES) unlike most of the studies. Tribocorrosion tests were performed to understand the effect of sliding wear on electrochemical potential and effect of electrochemical potential on the material loss of AISI 316 in SWE. Also, the tribological properties of AISI 316 stainless steel were investigated and COFs in SWE were determined under different electrochemical potentials. The microstructure and damage mechanisms were analysed using a scanning electron microscope (SEM), energy dispersive spectroscopy (EDS) and optical microscope images to determine surface condition and material loss of AISI 316 after tribocorrosion tests.

2. Materials and methods

The study comprised four main stages: Material preparation, tribocorrosion test, analysis and results. In the first stage, the size and surface preparation of the samples was carried out. At this stage, cutting, face turning, grinding, polishing, electric cable soldering and, finally bakelite operations of samples were performed. In the second stage, a sample was placed in the corrosion cell and filled after with seawater whose content was determined by ICP-OES method. The alumina ball was contacted with the sample inside the cell integrated on the tribometer. The potentiostat was used to record electrochemical data via electrodes placed inside the corrosion cell. After, SEM, EDS and optical microscope investigations of the tested samples were performed in the analysis stage. At this stage, COF, electrochemical data, wear track volume, microstructure, deformations and material transfer were evaluated. At the last stage, the results of the analyses and discussions were presented.

2.1. Preparation of specimens

In the experimental stage of this study, AISI 316 stainless steel specimens were employed. A 20 mm diameter AISI 316 stainless steel rod was cut into 10 mm thick samples then machined to 9 mm. Each specimen (Ø 20x9 mm) was ground until obtaining the mirror-like surface using SiC papers at different grit numbers such as 320, 800, 1200 respectively and then cleaned in acetone and ethanol. The surfaces of ground samples were polished in wet media using a 3 μm diamond suspension and 3 μm velvet felt in a water-based sample polishing device. In all stages of grinding and polishing processes, sample surfaces were cleaned in ethanol to avoid corrosion and contamination. To contact only the upper surfaces of specimens with the electrolyte, the rest of the surfaces were sealed using bakelite before being immersed into tribocorrosion cell. Thus, a 3.14 cm^2 area left in contact with electrolyte was provided to avoid corrosion interactions during the measurements. A copper cable with sheath was soldered to the back of the samples to record current and potential data. The chemical properties of AISI 316 material were given in Table 1.

2.2. Characterization

Surface and wear pattern of the samples were determined by SEM (TESCAN, MAIA3 XMU model) with EDS (OXFORD, X-Max model). Optical profilometry (HUVITZ, HDS-5800 model) was used to determine the cross-sectional area and volume of the wear tracks.

Elemental analysis performed by the method of ICP-OES (PERKIN ELMER OPTIMA 2100 DV model) of the natural seawater used in the experiments was given in Table 2. The salinity (NaCl) ratio of seawater taken from the Sea of Marmara was determined as 2.38%.

2.3. Corrosion and tribocorrosion test

Tribocorrosion experiments were conducted with a ball-on-disk reciprocating tribometer (Turkyus) integrated with the three-electrode potentiostat (Gamry, Interface 1000 model). A stroke frequency of 1.2 Hz (74 rpm), a normal load of 5 N, the reciprocating sliding stroke of 6 mm and total sliding (rubbing) time of 3600 s were applied in OCP measurement and potentiostatic polarisation tests. Alumina ball was preferred as the counter body with a diameter of 6 mm due to its high hardness, low electro-conductibility and noble characteristics in SWE. The reference electrode was a saturated calomel electrode (SCE), the counter electrode (CE) was platinum wire and the working electrode (WE) was AISI 316 samples in this study. All potentials were measured versus SCE. The corrosion cell produced from a polymer material (Delrin) to prevent corrosive effects was integrated into the tribometer. All the experiments were performed at 25 ± 1 °C. The experimental infrastructure and components used in the study were shown in Fig. 1.

OCP was recorded to monitor changes in electrochemical potential due to mechanical effects under loaded and unloaded conditions. The specimens were held in seawater for an hour before tribocorrosion tests to reach a steady OCP value. After that, the

Table 1
Chemical properties (wt%) of AISI 316.

Chemical composition (wt%)								
Cr	Ni	Mo	C	S	P	Si	Mn	Fe
17.2	10.2	2.1	0.04	<0.03	<0.045	<1.0	<2.0	Bal.

Table 2
Elemental analysis of natural seawater used in the experiments.

Ca	Mg	Na	K	S	Sr	SO_4
2.300 ppm	7.716 ppm	61.800 ppm	3.155 ppm	5.188 ppm	2.90 ppm	15.540 ppm

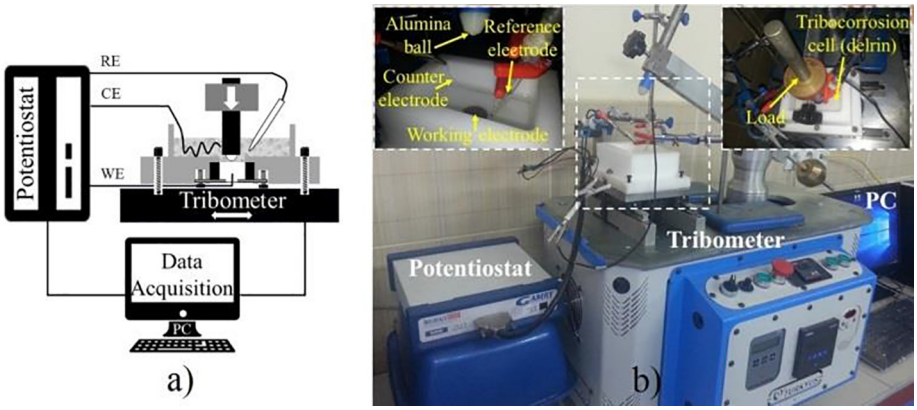

Fig. 1. Tribocorrosion experimental set-up used in the study: a) schematic of tribocorrosion system and test cell, b) laboratory setup.

tribocorrosion experiments were started. When determining OCP, unloaded potential value was measured in the first 30 min and then the rubbing was started. The samples were abraded for an hour against alumina ball. OCP and COF values were recorded during this time. After the rubbing period, the OCP was recorded for a further 30 min to achieve a stable potential value and the experiment was ended.

Potentiodynamic polarization tests were made at 1 mV/s scanning speed between potentials of −1 V and 2 V under both corrosion and tribocorrosion conditions to find out the corrosion kinetics of the AISI 316 material. Also, potentiostatic polarization tests were also performed to determine the effect of electrochemical potential on tribocorrosion behaviour and material losses of AISI 316 under different electrochemical conditions. The selected potentials were determined considering the potentiodynamic polarization curves to be within one of them in the anodic region and one of them in cathodic region. To determine the loss of material caused by only the wear effects, −1 V cathodic potential was chosen. Thus, the effect of corrosion was reduced to negligible levels with cathodic protection in tribocorrosion of AISI 316 steel in SWE. Cathodic protection could help to explain the contribution of pure mechanical wear and the total material loss in the wear track. Many researchers used a similar test procedure to get the measure of the mechanical wear component in tribocorrosion [35,47,48]. 0.3 V potential was selected to understand anodic dissolution in tribocorrosion of AISI 316 steel in SWE. The applied potentials were retained at a stable value during the tests with a suitable current between working and counter electrodes. The current was measured at these potentials as a function of time to monitor the development of the electrochemical kinetics of the related reactions [46]. In polarisation tests, the samples were abraded under 5 N loads for an hour as with the OCP.

2.4. Determination of material loss volume

Material losses from the wear tracks were found by multiplying track length and average transverse cross-section area of the wear track which was obtained from the optical microscope. Three measurements were taken from the mutual points of each sample and the average value of these measurements was used to obtain the average cross-section area of the wear track.

3. Results and discussions

3.1. Effect of sliding contact on electrochemical potential

Tribocorrosion tests were carried out to determine the effect of the sliding contact on the electrochemical potential under OCP conditions. OCP of the samples, which were kept in seawater for an hour before the tribocorrosion test, reached a stable value of around 20 mV at the end of the 1800 s under unloaded conditions according to Fig. 2. Thereafter, rubbing initialised under 5 N loads and OCP abruptly dropped to around −70 mV at this instant. Garcia et al. and Henry et al. explained that the deterioration of passive film with mechanical effects caused the sudden drop in OCP. Therefore, OCP shifted to more cathodic values as in previous studies when the rubbing started [20,21]. The wear process was finished in an hour. At the end of the wear period, the decrease in the potential continued and finally reached −104 mV at 5400 s,

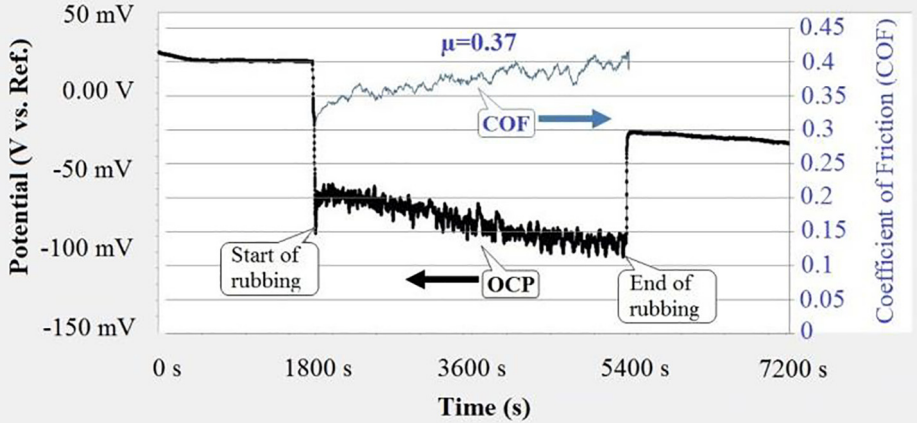

Fig. 2. Evaluation of OCP and COF in tribocorrosion test.

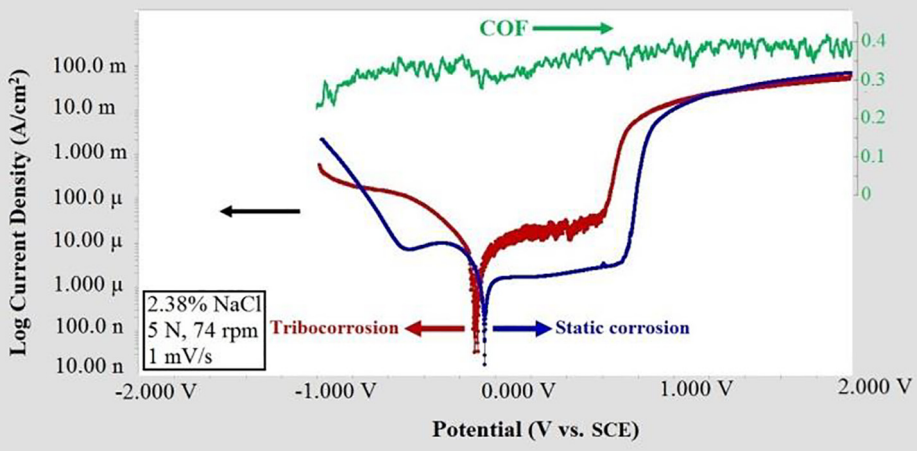

Fig. 3. Potentiodynamic polarization scans under corrosion and tribocorrosion conditions.

according to Fig. 2. OCP sharply increased at the end of 5400 s by the termination of the rubbing. The results pointed out passive oxide film re-formation in the wear zone, according to Berradja et al. [40]. However, OCP could not reach its original value before rubbing period because of the deformed surface. The superimposed graph of COF with OCP was also given in Fig. 2. According to Fig. 2, COF increased continuously over time, while OCP decreased. The average value of COF was determined as 0.37.

Potentiodynamic polarization curves of the AISI 316 in SWE between – 1 V (SCE) and 2 V potentials under both corrosion and tribocorrosion (5 N loaded) conditions were given in Fig. 3. There were significant differences in the polarisation behaviour of AISI 316 steel between static corrosion and tribocorrosion

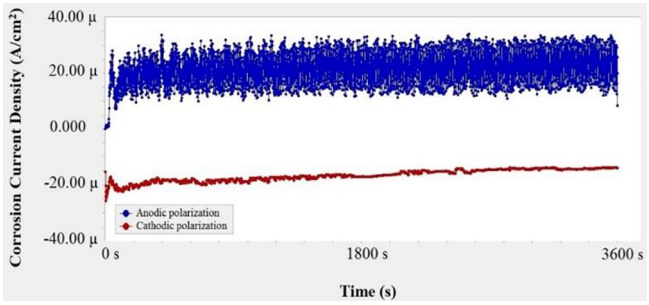

Fig. 4. Corrosion current densities under anodic (0.3 V) and cathodic polarization (-1 V) conditions.

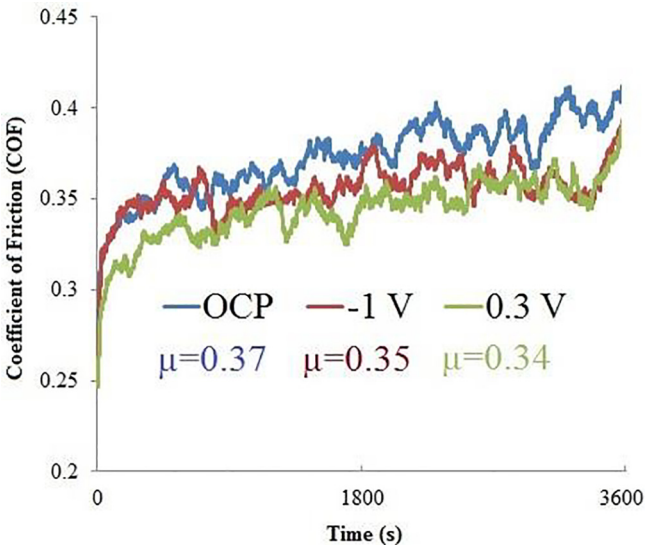

Fig. 5. Evaluation of COF under different electrochemical potentials.

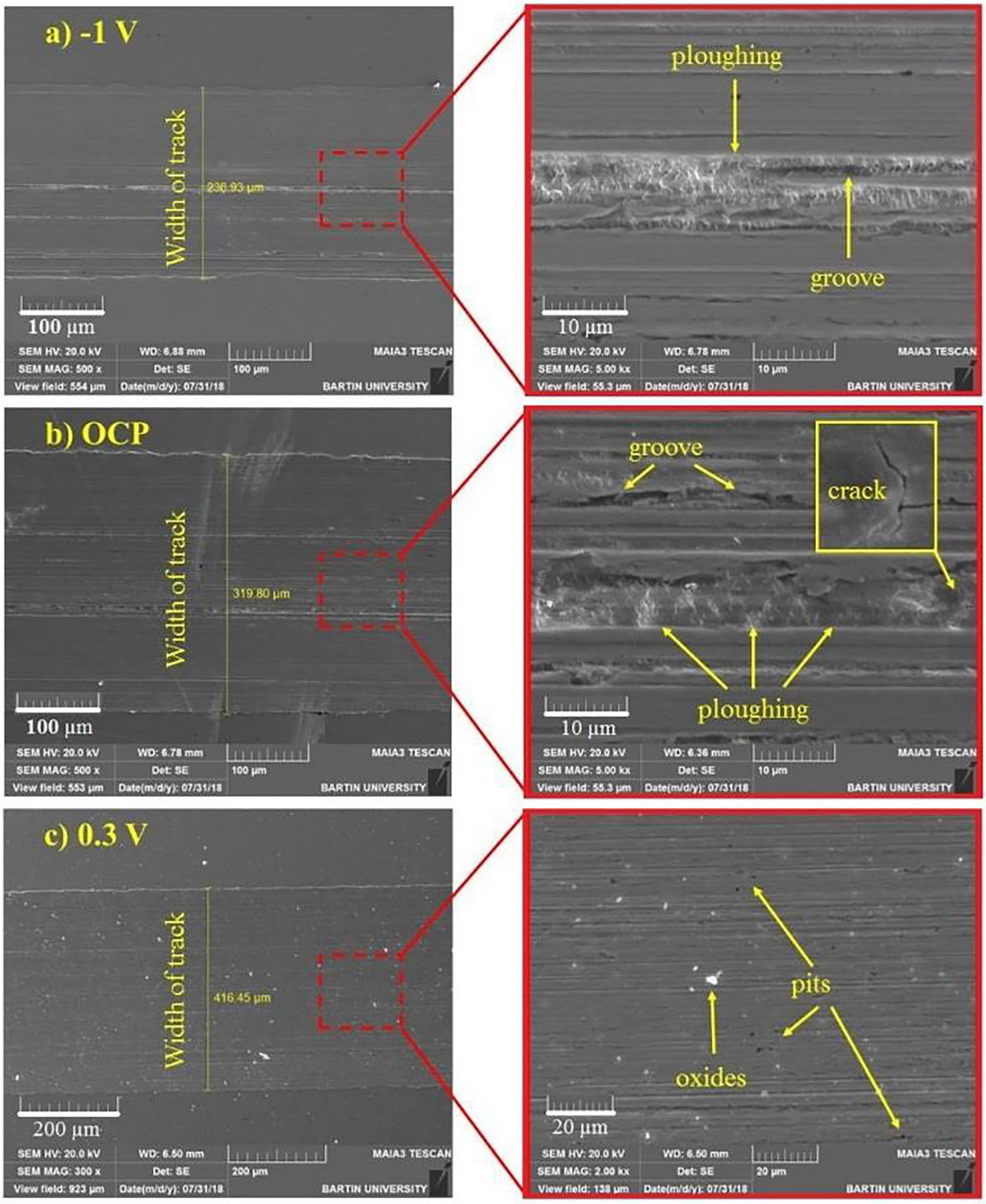

Fig. 6. SEM analysis of AISI 316 specimens after tribocorrosion experiments: a) −1 V, b) OCP, c) 0.3 V.

conditions. According to Fig. 3, the corrosion potential under tribocorrosion condition was − 106 mV, and that was lower than the static corrosion condition (−79 mV). This was a sign that the wear effects reduce the corrosion potential. The reported literature was consistent with the results [21,22]. Fig. 3 showed that the corrosion potential shifted to a more cathodic potential while corrosion current density increased. The corrosion current density increased in tribocorrosion condition because of exposing the fresh metal surface to the solution by rubbing [42]. However, the fluctuations in the current density under the tribocorrosion condition which was seen in Fig. 3 was attributed to de-passivation products generated by wear [41,42]. Tang et al. and Hacisalihoglu et al. observed similar findings for different passive metals such as titanium alloy and stainless steel in their studies. The passive zone in the potentiodynamic curve in tribocorrosion conditions constricted slightly according to corrosion conditions. The delamination of the passive film in the wear track caused the formation of galvanic coupling between the bare metal surface and the passive (unworn) surface [43]. Besides, the risk of pitting corrosion, which constitutes the weak point of the stainless steels in the SWE, was arisen in potentiodynamic scans. Different researchers confirmed that galvanic coupling formation will cause the high corrosion potential

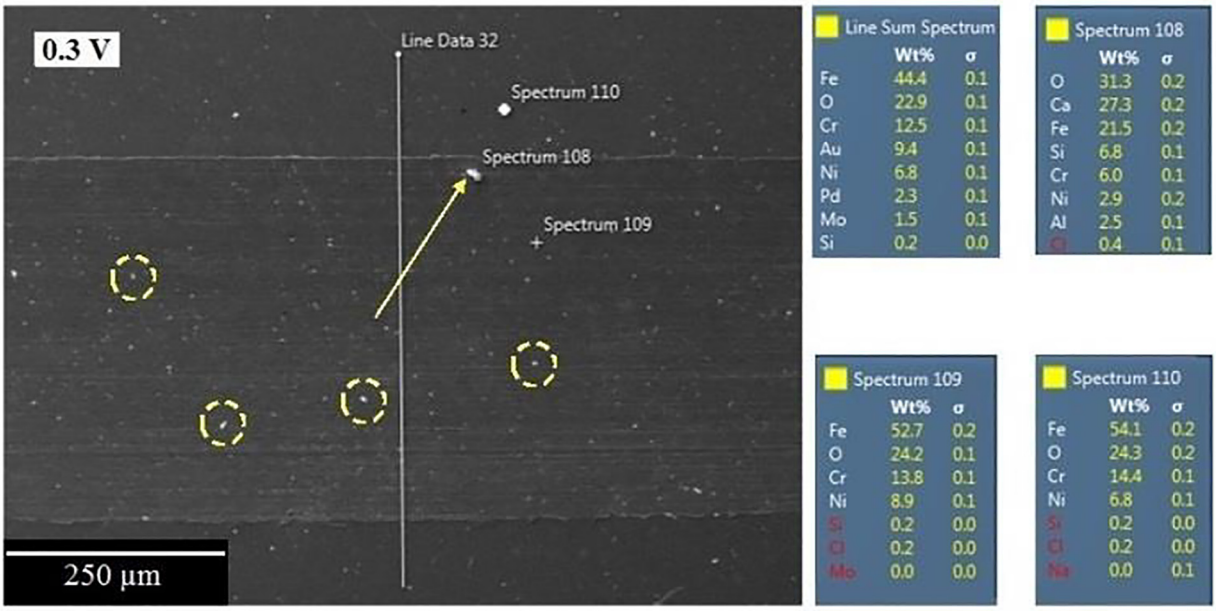

Fig. 7. EDS line spectrum: Cl and Na ion determination in the wear track.

between worn and unworn zones and this will increase anodic dissolution and pitting [13,25].

Developments of COF were recorded during potentiodynamic polarization measurements under sliding conditions. Fig. 3 also showed the correlation between COF and the corrosion current density. COF diminished slightly to about 0.3 near OCP, however re-increased after crossing to the anodic region as in Fig. 3. Ismail et al. [44] reported similar findings of friction changes depending on potential under potentiodynamic polarisation conditions in tribocorrosion. These results showed that developing oxide film could reduce COF in the passive region. Third body formation from both wear particle of AISI 316 and the degradation of alumina in the anodic region may cause a relatively high COF [45].

3.2. Effect of electrochemical potential on friction behaviour

Potentiostatic polarization tests were performed under −1 V and 0.3 V potentials to determine the effect of electrochemical potential on friction behaviour and material loss of AISI 316 stainless steel. The evolution of the corrosion current density in anodic and cathodic polarization during the tribocorrosion experiments in natural SWE for AISI 316 were presented in Fig. 4. According to Fig. 4, the abrasion of the metal surface and thereafter delamination of the passive film covering the surface caused a sharp increase in the corrosion current density at the beginning of the potentiostatic test conducted under 0.3 V potential. Corrosion current density in the potentiostatic tests under 0.3 V anodic potential was at positive values of about 20μA/cm2 during the test. The corrosion current density was at negative values of about (−20) μA/cm^2 during the potentiostatic test conducted under −1 V that was an indication of achieving the cathodic protection successfully.

Fig. 5 showed the developments and average values of COFs under OCP and different potentiostatic potentials. The lowest COF (0.34) was obtained under anodic potential as seen in Fig. 5. The main reason for this was the reduction of the contact area because of forming the pits (Fig. 6) and oxides (Fig. 7) in the wear zone. Obadele et al. confirmed that pits and oxides in the wear zone could provide a lubricating effect on the surface of AISI 310 and AISI 316 grade steel in 3.5% NaCl solution [23]. The average COF value (0.35) under −1 V cathodic protection was observed less than under OCP conditions (0.37) because only the wear effects occurred. According to Fig. 5, COF has a similar increasing trend over time in all three potentials. This originated from a few adhesive and mainly abrasive contacts (Fig. 9) between the surface of the substrate and the counter body. Also, exposure to the fresh surface of the metal to the electrolyte caused an increase in friction because of corrosion products [49].

3.3. Surface morphology and analysis

After each tribocorrosion experiment conducted under potentiostatic and OCP conditions, changes in surface morphology were analysed by SEM, EDS and optical microscope. Plastic flow indications were observed such as scratches, ploughing, micro-cracks, material detachment and folding in the wear tracks. The structures of the wear tracks, as well as the width and depth of the tracks obtained from the SEM, were examined. It was determined that the width and depth of the wear tracks (the volume of the wear tracks) increased from the cathodic potential towards the anodic potential (Figs. 6 and 10).

The surface analysis of the abraded specimen after tribocorrosion test, which was done under −1 V cathodic potential, showed that there was no pit formation or any other form of corrosion on the surface. Since only the wear effects were observed under cathodic potential, effects of the rubbing on the wear track were more pronounced than corrosion effects. In Fig. 6a, many nearly parallel ploughing and grooves were determined in the wear track after tribocorrosion test which was conducted under −1 V cathodic potential. In experiments performed under OCP, micro-cracks were detected in the wear track, according to Fig. 6b. Bateni et al. confirmed the formation of cracks on the worn surfaces in their study and attributed the formation of cracks to the galvanic cells [50]. It was reported by different researchers [16,51–53] that these micro-cracks acted as a diffusion channel and the leakage of Cl ions into these micro-cracks could accelerate general corrosion with pitting. Na and Cl ions were also detected in this study in micro-cracks and

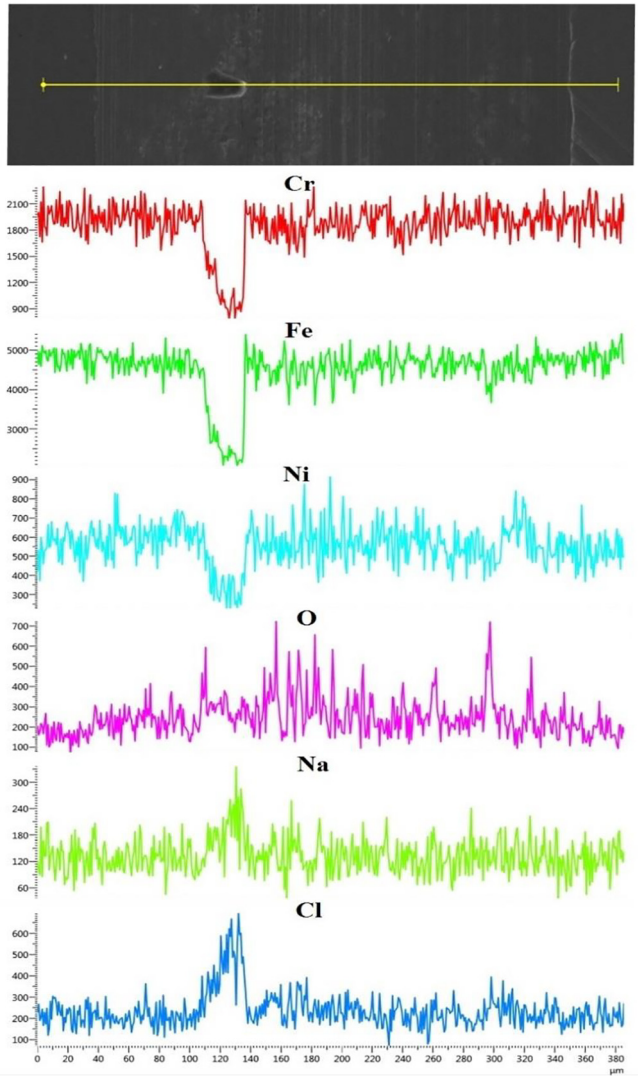

Fig. 8. EDS analysis of oxides in the wear track after 0.3 V potentiostatic tribocorrosion test.

pits by EDS spectrum analysis, according to Fig. 8. In Fig. 8, amount of the Fe, Cr, Ni elements decreased between 120 µm and150 µm in the cross-sectional EDS line spectrum of the wear track while the amount of Na and Cl ions increased in the same interval. Hence, the potential of Cl ions caused pitting corrosion and penetration into micro-cracks was revealed. According to Fig. 6c, pits were also observed in the wear track at 0.3 V potential and corrosion effects were observed more pronounced.

Na and Cl ions detected in the wear tracks could cause corrosion products on the surface. Pits (Fig. 6c) and oxide formations (Fig. 7) were detected in SEM and EDS analysis of the wear track after tribocorrosion tests conducted under the 0.3 V potential. In Fig. 7, the oxides were defined with the highest element weight ratio (31.3%) of Oxygen (O) in Spectrum 108. However, the other oxides dispersed in the wear track were also circled in Fig. 7. Oxygen also has the second-highest weight ratio in all other spectrums (Line sum, 109 and 110), according to Fig. 7. Oxide layer formation on the surface created an intermediate layer and reduced the COF at the anodic potential [50]. The reduction of the contact area between alumina and AISI 316 due to pits and also lubrication effect of the oxides provided the lowest COF at 0.3 V potential [54]. Cl ions were detected at very low levels in the point spectrum at 0.3 V potential, according to Fig. 7.

3.4. Material loss from wear track

Interaction between wear and corrosion, known as synergy, strongly influences material losses in tribocorrosion. Changes in electrochemical potential can trigger damage or even complete removal of the passive film on the contact surface. In this case, wear-induced corrosion or corrosion-induced wear can be dominant in tribocorrosion [24].

In Fig. 9a, pure mechanical effects were observed such as ploughing and sharp scratching in and the edge of the wear track. The adhesion took place at local points of the wear track. Stick-slip behaviour between the substrate and the counter face contacting to each other caused the material detachment. Material detachments in the wear track pointed out adhesive wear for local points as seen in Figs. 9b and 9c. Many pits were determined in the wear track at 0.3 V potential and also a pit cluster was detected around the edge of the wear track in Fig. 9c which undergo corrosion.

Fig. 10 showed the wear track structures comparatively. Fig. 10 showed the wear track structures comparatively. According to Fig. 10, a narrow and superficial track structure formed at −1 V and a wider and deeper track structure at 0.3 V compared with at OCP. Material loss volumes under different potentials were found as 0.00003 mm^3 at −1 V, 0.00040 mm^3 at OCP and 0.00051 mm^3 at 0.3 V in Fig. 10. Moreover, AISI 316 presented 17 times more material loss in the tribocorrosion test at 0.3 V than −1 V.

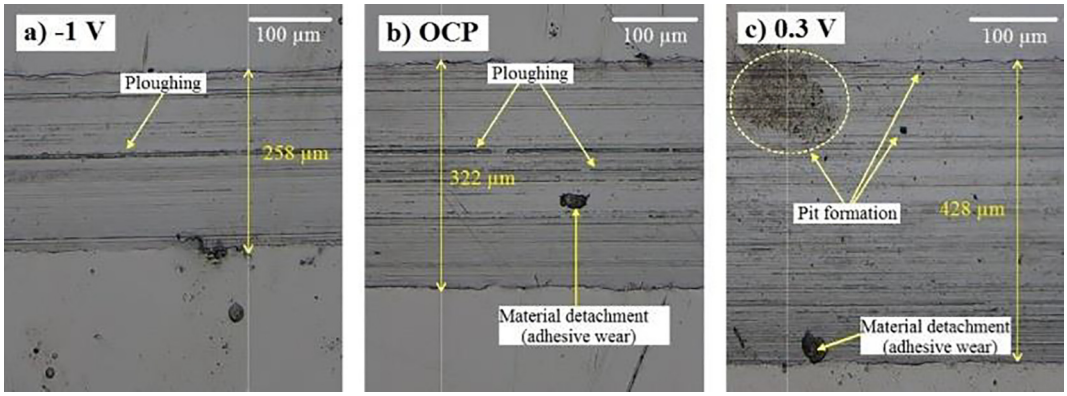

Fig. 9. Optical micrograph views of wear tracks under different potentials: a) −1 V, b) OCP, c) 0.3 V.

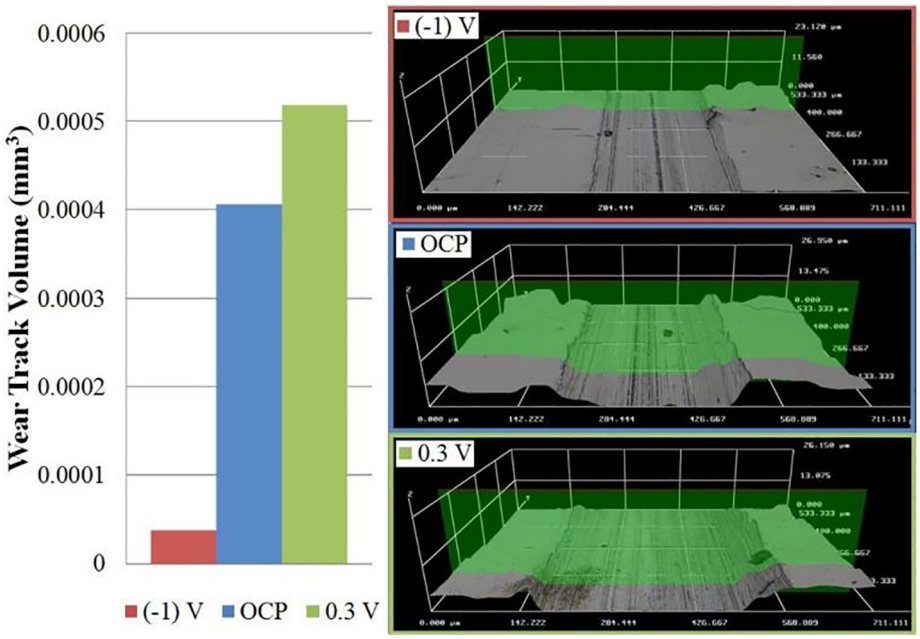

Fig. 10. Wear track volume under different electrochemical potentials.

4. Conclusions

In this study, the effects of sliding wear and electrochemical potential on tribocorrosion behaviour of the AISI 316 stainless steel in natural SWE were investigated. Based on the experiments, the following results were summarised:

1. The deterioration of oxide film in the wear track by the mechanical effects resulted in a cathodic shift in the OCP. The disappearance of rubbing effects provided the re-passivation and potential increase in corrosion.
2. The lowest COF value was obtained as 0.34 at 0.3 V anodic potential. This result was attributed to pit formation which caused a reduced contact surface and to the oxides with the lubrication effect in the wear track. COF values were 0.37 and 0.35 at OCP and −1 V, respectively.
3. Corrosion potential and corrosion current density in potentiodynamic scans under tribocorrosion conditions were lower than under static corrosion conditions. In potentiodynamic scans, mechanical effects have decreased the corrosion potential.
4. Ploughing, material detachment and micro-cracks were detected in SEM images of the wear tracks after tribocorrosion tests were conducted under OCP and −1 V potential. Galvanic effects between the wear track and unworn areas caused cracks in the surface at OCP. Cl ions detected in the EDS analysis accelerated corrosion and pitting in micro-cracks.
5. Material losses from the wear tracks increased from the cathodic potential towards the anodic potential. The lowest wear track volume (0.00003 mm3) was obtained under −1 V cathodic potential. AISI 316 exhibited 17 times more material loss from the wear track at 0.3 V potential than −1 V potential in tribocorrosion tests.

Declaration of Competing Interest

The authors declare that they have no known competing financial interests or personal relationships that could have appeared to influence the work reported in this paper.

Acknowledgments

This experimental study was supported by Scientific Research Projects Coordination Unit of Bartın University (Project Number: 2017- FEN CD-02), Turkey.

References

[1] S. Mischler, Triboelectrochemical techniques and interpretation methods in tribocorrosion: A comparative evaluation, Tribol. Int. 41 (2008) 573–583, https://doi.org/10.1016/j.triboint.2007.11.003.
[2] D. Landolt, S. Mischler, Tribocorrosion of passive metals and coatings, Woodhead Publishing, 2011.
[3] A. López-Ortega, R. Bayón, J.L. Arana, Evaluation of protective coatings for offshore applications. Corrosion and tribocorrosion behavior in synthetic seawater, Surf. Coatings Technol. 349 (2018) 1083–1097, https://doi.org/10.1016/j.surfcoat.2018.06.089.
[4] N.P. Brandon, R. Wood, The influence of interfacial potential on friction and wear in an aqueous drilling mud, Wear. 170 (1993) 33–38, https://doi.org/10.1016/0043-1648(93)90348-P.
[5] R.J.K. Wood, A.S. Bahaj, S.R. Turnock, L. Wang, M. Evans, Tribological design constraints of marine renewable energy systems, Philos. Trans. R. Soc. A Math. Phys. Eng. Sci. 368 (2010) 4807–4827, https://doi.org/10.1098/rsta.2010.0192.
[6] J. Cibulka, M.K. Ebbesen, G. Hovland, K.G. Robbersmyr, M.R. Hansen, A review on approaches for condition based maintenance in applications with induction machines located offshore, Model. Identif. Control. 33 (2012) 69–86, https://doi.org/10.4173/mic.2012.2.4.
[7] S.R. Schmid, K.J. Schmid, Marine equipment tribology, in: Mod. Tribol. Handb. Vol. One Princ. Tribol., 2000: pp. 1371–1384.
[8] A. López, R. Bayón, F. Pagano, A. Igartua, A. Arredondo, J.L. Arana, J.J. González, Tribocorrosion behaviour of mooring high strength low alloy steels in synthetic seawater, Wear. 338–339 (2015) 1–10, https://doi.org/10.1016/j.wear.2015.05.004.
[9] S.S. Rajahram, T.J. Harvey, R. Wood, Erosion-corrosion resistance of engineering materials in various test conditions, Wear. 267 (2009) 244–254, https://doi.org/10.1016/j.wear.2009.01.052.
[10] Fan Aiming, Long Jinming, Tao Ziyun, An investigation of the corrosive wear of stainless steels in aqueous slurries, Wear. 193 (1996) 73–77, https://doi.org/10.1016/0043-1648(95)06684-5.
[11] X. Hu, A. Neville, An examination of the electrochemical characteristics of two stainless steels (UNS S32654 and UNS S31603) under liquid-solid impingement, Wear. 256 (2004) 537–544, https://doi.org/10.1016/S0043-1648(03)00563-5.
[12] P.A. Dearnley, G. Aldrich-Smith, Corrosion-wear mechanisms of hard coated austenitic 316L stainless steels, Wear. 256 (2004) 491–499, https://doi.org/10.1016/S0043-1648(03)00559-3.
[13] D. Landolt, Electrochemical and materials aspects of tribocorrosion systems, J. Phys. D. Appl. Phys. 39 (2006) 3121–3127, https://doi.org/10.1088/0022-3727/39/15/S01.

[14] R. Wood, Marine wear and tribocorrosion, Wear. 376–377 (2017) 893–910, https://doi.org/10.1016/j.wear.2017.01.076.
[15] W. Litwin, Water-lubricated bearings of ship propeller shafts - Problems, experimental tests and theoretical investigations, Polish Marit. Res. 16 (2009) 41–49, https://doi.org/10.2478/v10012-008-0055-z.
[16] J. Bhandari, F. Khan, R. Abbassi, V. Garaniya, R. Ojeda, Modelling of pitting corrosion in marine and offshore steel structures - A technical review, J. Loss Prev. Process Ind. 37 (2015) 39–62, https://doi.org/10.1016/j.jlp.2015.06.008.
[17] J.-P. Celis, P. Ponthiaux, Testing tribocorrosion of passivating materials supporting research and industrial innovation : Testing tribocorrosion of passivating materials supporting research and industrial innovation, 2012.
[18] C.O. Olsson, D. Landolt, Passive films on stainless steels - Chemistry, structure and growth, Electrochim. Acta. 48 (2003) 1093–1104, https://doi.org/10.1016/S0013-4686(02)00841-1.
[19] Y. Tsutsumi, A. Nishikata, T. Tsuru, Pitting corrosion mechanism of Type 304 stainless steel under a droplet of chloride solutions, Corros. Sci. 49 (2007) 1394–1407, https://doi.org/10.1016/j.corsci.2006.08.016.
[20] I. García, D. Drees, J.P. Celis, Corrosion-wear of passivating materials in sliding contacts based on a concept of active wear track area, Wear. 249 (2001) 452–460, https://doi.org/10.1016/S0043-1648(01)00577-4.
[21] P. Henry, J. Takadoum, P. Berçot, Depassivation of some metals by sliding friction, Corros. Sci. 53 (2011) 320–328, https://doi.org/10.1016/j.corsci.2010.09.038.
[22] N. Diomidis, J.P. Celis, P. Ponthiaux, F. Wenger, Tribocorrosion of stainless steel in sulfuric acid: Identification of corrosion-wear components and effect of contact area, Wear. 269 (2010) 93–103, https://doi.org/10.1016/j.wear.2010.03.010.
[23] B.A. Obadele, A. Andrews, M.B. Shongwe, P.A. Olubambi, B. Abiodun, A. Andrews, M. Brendon, P. Apata, B.A. Obadele, A. Andrews, M.B. Shongwe, P.A. Olubambi, Tribocorrosion behaviours of AISI 310 and AISI 316 austenitic stainless steels in 3.5% NaCl solution, Mater. Chem. Phys. 171 (2015) 239–246, https://doi.org/10.1016/j.matchemphys.2016.01.013.
[24] J. Chen, Q. Zhang, Q.A. Li, S.L. Fu, J.Z. Wang, Corrosion and tribocorrosion behaviors of AISI 316 stainless steel and Ti6Al4V alloys in artificial seawater, Trans. Nonferrous Met. Soc. China (English Ed. 24 (2014) 1022–1031, https://doi.org/10.1016/S1003-6326(14)63157-5.
[25] P. Ponthiaux, F. Wenger, D. Drees, J.P. Celis, Electrochemical techniques for studying tribocorrosion processes, Wear. 256 (2004) 459–468, https://doi.org/10.1016/S0043-1648(03)00556-8.
[26] M. Stemps, S. Mischler, D. Landolt, M. Stemp, S. Mischler, D. Landolt, The effect of contact configuration on the tribocorrosion of stainless steel in reciprocating sliding under potentiostatic control, Corros. Sci. 45 (2003) 625–640, https://doi.org/10.1016/S0010-938X(02)00136-1.
[27] X. Hu, A. Neville, The electrochemical response of stainless steels in liquid-solid impingement, in: Wear, 2005: pp. 641–648. doi:10.1016/j.wear.2004.09.043.
[28] M. Stemp, S. Mischler, D. Landolt, Electrochemical aspects of tribocorrosion, Tribol. Ser. 39 (2001) 539–547, https://doi.org/10.1016/S0167-8922(01)80137-1.
[29] M. Stemp, S. Mischler, D. Landolt, The effect of mechanical and electrochemical parameters on the tribocorrosion rate of stainless steel in sulphuric acid, Wear. 255 (2003) 466–475, https://doi.org/10.1016/S0043-1648(03)00085-1.
[30] P. Jemmely, S. Mischler, D. Landolt, Electrochemical modeling of passivation phenomena in tribocorrosion, Wear. 237 (2000) 63–76, https://doi.org/10.1016/S0043-1648(99)00314-2.
[31] E. Liu, Y. Zhang, L. Zhu, Z. Zeng, R. Gao, Effect of strain-induced martensite on the tribocorrosion of AISI 316L austenitic stainless steel in seawater, RSC Adv. 7 (2017) 44923–44932, https://doi.org/10.1039/C7RA07318F.
[32] Y. Zhang, J.Z. Wang, X.Y. Yin, F.Y. Yan, Tribocorrosion behaviour of 304 stainless steel in different corrosive solutions, Mater. Corros. 67 (2016) 769–777, https://doi.org/10.1002/maco.201508641.
[33] J. Chen, F.Y. Yan, B.B. Chen, J.Z. Wang, Assessing the tribocorrosion performance of Ti-6Al-4V, 316 stainless steel and Monel K500 alloys in artificial seawater, Mater. Corros. 64 (2013) 394–401, https://doi.org/10.1002/maco.201106249.
[34] Y.N. Kok, R. Akid, P.E. Hovsepian, Tribocorrosion testing of stainless steel (SS) and PVD coated SS using a modified scanning reference electrode technique, Wear. 259 (2005) 1472–1481, https://doi.org/10.1016/j.wear.2005.02.049.
[35] S.W. Watson, F.J. Friedersdorf, B.W. Madsen, S.D. Cramer, Methods of measuring wear-corrosion synergism, Wear. 181–183 (1995).
[36] F. Assi, H. Bohni, Study of wear – corrosion synergy with a new microelectrochemical, Wear. 233235 (1999) 505–514. www.elsevier.comrlocaterwear.
[37] S. Mischler, D. Landolt, Wear-accelerated corrosion of passive metals in tribocorrosion systems, J. Electrochem. Soc. 145 (1998) 750, https://doi.org/10.1149/1.1838341.
[38] D. Landolt, S. Ischler, M. Stemp, Electrochemical methods in tribocorrosion: a critical appraisal, Electrochim. Acta. 46 (2001) 3913–3929, https://doi.org/10.1016/S0013-4686(01)00679-X.
[39] D. Holmes, S. Sharifi, M.M. Stack, Tribo-corrosion of steel in artificial saliva, Tribol. Int. 75 (2014) 80–86, https://doi.org/10.1016/j.triboint.2014.03.007.
[40] A. Berradja, F. Bratu, L. Benea, G. Willems, J.P. Celis, Effect of sliding wear on tribocorrosion behaviour of stainless steels in a Ringer's solution, Wear. 261 (2006) 987–993, https://doi.org/10.1016/j.wear.2006.03.003.
[41] Y. Tang, Y. Zuo, J. Wang, X. Zhao, B. Niu, B. Lin, The metastable pitting potential and its relation to the pitting potential for four materials in chloride solutions, Corros. Sci. 80 (2014) 111–119, https://doi.org/10.1016/j.corsci.2013.11.015.
[42] I. Hacisalihoglu, A. Samancioglu, F. Yildiz, G. Purcek, A. Alsaran, Tribocorrosion properties of different type titanium alloys in simulated body fluid, Wear. 332–333 (2014) 1–8, https://doi.org/10.1016/j.wear.2014.12.017.
[43] B. Abiodun, A. Andrews, M. Brendon, P. Apata, Tribocorrosion behaviours of AISI 310 and AISI 316 austenitic stainless steels in 3. 5 %, NaCl solution 171 (2016) 239–246.
[44] M.N.F. Ismail, T.J. Harvey, J.A. Wharton, R.J.K. Wood, A. Humphreys, Surface potential effects on friction and abrasion of sliding contacts lubricated by aqueous solutions, Wear. 267 (2009) 1978–1986, https://doi.org/10.1016/j.wear.2009.06.007.
[45] D. Landolt, S. Mischler, M. Stemp, S. Barril, Third body effects and material fluxes in tribocorrosion systems involving a sliding contact, Wear. 256 (2004) 517–524, https://doi.org/10.1016/S0043-1648(03)00561-1.
[46] K.C. Tekin, U. Malayoglu, Assessing the tribocorrosion performance of three different nickel-based superalloys, Tribol. Lett. 37 (2010) 563–572, https://doi.org/10.1007/s11249-009-9552-1.
[47] C. Moosbrugger, P. Editor, G.J. Anton, E. Assistant, N. Hrivnak, J. Kinson, C. Polakowski, P. Editors, K. Muldoon, P. Assistant, M. Park, ASM Handbook π Volume 13A Corrosion : Fundamentals , Testing , and Protection, 13 (2003).
[48] Y. Sun, R. Bailey, Improvement in tribocorrosion behavior of 304 stainless steel by surface mechanical attrition treatment, Surf. Coatings Technol. 253 (2014) 284–291, https://doi.org/10.1016/j.surfcoat.2014.05.057.
[49] E. Huttunen-Saarivirta, L. Kilpi, T.J. Hakala, L. Carpen, H. Ronkainen, Tribocorrosion study of martensitic and austenitic stainless steels in 0.01M NaCl solution, Tribol. Int. 95 (2016) 358–371, https://doi.org/10.1016/j.triboint.2015.11.046.
[50] M.R. Bateni, J.A. Szpunar, X. Wang, D.Y. Li, Wear and corrosion wear of medium carbon steel and 304 stainless steel, Wear. 260 (2006) 116–122, https://doi.org/10.1016/j.wear.2004.12.037.
[51] P. Leroux, Tribocorrosion on Diamond Like Carbon, (2015). doi:10.13140/RG.2.1.2169.7444.
[52] Y. Zhang, X. Yin, F. Yan, Effect of halide concentration on tribocorrosion behaviour of 304SS in artificial seawater, Corros. Sci. 99 (2015) 272–280, https://doi.org/10.1016/j.corsci.2015.07.017.
[53] Q. Chen, Y. Cao, Z. Xie, T. Chen, Y. Wan, H. Wang, X. Gao, Y. Chen, Y. Zhou, Y. Guo, Tribocorrosion behaviors of CrN coating in 3.5 wt% NaCl solution, Thin Solid Films. 622 (2016) 41–47, https://doi.org/10.1016/j.tsf.2016.12.023.
[54] Y. Sun, V. Rana, Tribocorrosion behaviour of AISI 304 stainless steel in 0.5M NaCl solution, Mater. Chem. Phys. 129 (2011) 138–147, https://doi.org/10.1016/j.matchemphys.2011.03.063.